Title	Atomic structure of recombinant thaumatin II reveals flexible conformations in two residues critical for sweetness and three consecutive glycine residues.
Author(s)	Masuda, Tetsuya; Mikami, Bunzo; Tani, Fumito
Citation	Biochimie (2014), 106: 33-38
Issue Date	2014-11
URL	http://hdl.handle.net/2433/203009
Right	© 2014. This manuscript version is made available under the CC-BY-NC-ND 4.0 license http://creativecommons.org/licenses/by-nc-nd/4.0/
Type	Journal Article
Textversion	author

Atomic structure of recombinant thaumatin II reveals flexible conformations in two residues critical for sweetness and three consecutive glycine residues.

Tetsuya Masuda,[a]* Bunzo Mikami,[b] Fumito Tani[a]

[a]***Division of Food Science and Biotechnology,***

[b]***Division of Applied Life Sciences,***

Graduate School of Agriculture, Kyoto University,

Gokasho, Uji, Kyoto, 611-0011, Japan

*Corresponding author

Division of Food Science and Biotechnology,

Graduate School of Agriculture, Kyoto University,

Uji, Kyoto 611-0011, Japan Tel.: +81-774-38-3741; Fax: +81-774-38-3740

E-mail: mailto:t2masuda@kais.kyoto-u.ac.jp

Abstract

Thaumatin, an intensely sweet-tasting protein used as a sweetener, elicits a sweet taste at 50 nM. Although two major variants designated thaumatin I and thaumatin II exist in plants, there have been few dedicated thaumatin II structural studies and, to date, data beyond atomic resolution had not been obtained. To identify the detailed structural properties explaining why thaumatin elicits a sweet taste, the structure of recombinant thaumatin II was determined at the resolution of 0.99 Å. Atomic resolution structural analysis with riding hydrogen atoms illustrated the differences in the direction of the side-chains more precisely and the electron density maps of the C-terminal regions were markedly improved. Though it had been suggested that the three consecutive glycine residues (G142-G143-G144) have highly flexible conformations, G143, the central glycine residue was successfully modelled in two conformations for the first time. Furthermore, the side chain r.m.s.d. values for two residues (R67 and R82) critical for sweetness exhibited substantially higher values, suggesting that these residues are highly disordered. These results demonstrated that the flexible conformations in two critical residues favoring their interaction with sweet taste receptors are prominent features of the intensely sweet taste of thaumatin.

Keywords: Thaumatin; Sweet-tasting protein; Shelxl; Flexible conformations; Atomic resolution

1. Introduction

Thaumatin is the one of the sweetest proteins known and is used as a low-calorie sugar substitute as well as for medical purposes for life style-related diseases such as hypertension, hyperlipidemia, diabetes and obesity. It is nearly 100,000 times sweeter than sucrose on a molar basis and elicits a sweet taste sensation at 50 nM in humans [1]. The intensely sweet sensation of thaumatin could be useful for revealing the interaction with sweet taste receptors. Sweet-tasting proteins are too large to fit the cavity of the interaction sites for small sweeteners, and activation of the sweet receptor by sweet-tasting proteins seems to occur in a different manner [2-5].

Thaumatin is frequently used in crystallization studies and, to date, more than 75 structures have been deposited in the Protein Data Bank. Most of them are derived from plant sources, and no further purification tends to be performed for crystallization although plant-sourced thaumatin includes some variants. Since structural information on the charge distribution and protonation state of hydrogen atoms would be useful for understanding the elicitation of the sweetness of thaumatin as well as the interaction with sweet receptors, high-resolution x-ray crystal analysis and neutron crystallographic studies have been conducted [6-10]. Atomic resolution structures with hydrogen atoms of recombinant thaumatin I (1.0-1.1 Å) as well as purified plant thaumatin I (0.94 Å) demonstrated that electron density maps of some

residues were significantly improved to clarify subtle structural variations among thaumatin variants [6, 7]. Furthermore, comparisons of structures at atomic resolution revealed the large disulfide-rich region in domain II to be sensitive to a pH change [8]. Thus the structures of thaumatin I have been examined extensively, whereas little attention has been paid to thaumatin II. Thaumatin I differed from thaumatin II at four positions (N46K, S63R, K67R, and R76Q). The threshold values of sweetness of thaumatin I and thaumatin II are around 50 nM. Despite four amino acid differences between thaumatin I and II, the crystals of plant thaumatin II are very small and their reflections are limited to the resolution of 1.27 Å [11]. Detailed structural properties of thaumatin II, including hydrogen atoms, are still unknown and the effects of other residues adjacent to the two residues at positions 67 and 82 have not been examined yet. Atomic resolution of the structures of thaumatin with riding hydrogen atoms would provide the detailed structural features of thaumatin and give more valuable insight into the mechanism of the interaction with sweet receptors.

In the present study, the structure of recombinant thaumatin II was determined at a resolution of 0.99 Å. The model including hydrogen atoms was refined to an $R1$ of 9.74% for 140,800 reflections and 9.16% for 128,395 reflections with $Fo > 4\sigma(Fo)$ in the range 10-0.99 Å

2. Materials and methods

2.1. Materials

DH5α Quick competent cells were purchased from Toyobo Co., Ltd. (Osaka, Japan). *Pichia pastoris* X-33 was obtained from Invitrogen (Carlsbad, CA, USA). pCR®2.1-TOPO® and plasmid pPIC6αA were from Invitrogen. *E. coli* was cultured in LB Broth Miller or LB broth Lennox (Becton Dickinson, Sparks, MD, USA) and *P. pastoris* was grown in YPD medium or buffered minimal glycerol (BMG). KOD plus polymerase and LA Taq polymerase was from Toyobo and Takara Bio, Inc. (Shiga, Japan). Restriction enzymes were purchased from New England Biolabs Inc. (Beverly, MA, USA) and Toyobo. All other chemicals were of guaranteed reagent grade for biochemical use.

2.2. Cloning, expression and purification of recombinant thaumatin II

The mRNA was purified from a fruit of *Thaumatococcus daniellii* and first-strand cDNA was synthesized as described previously [12]. The thaumatin II gene containing the pre-sequence was amplified by PCR using the first-strand cDNA as a template, and 5'-GAATTCGAAATGGCCGCCACCACTTGCTTC-3' and 5'-TGCTCTAGA TTAGGCAGTAGGGCAGAAAGT-3' by KOD plus polymerase. The blunt-end PCR products were purified and then incubated with LA Taq

polymerase at 72°C for 30 min. PCR products having a single deoxyadenosine overhanging at the 3' end were immediately ligated into the pCR®2.1-TOPO® vector. The DNA sequence of the cloned thaumatin II gene was confirmed by an ABI 310 DNA sequencer (Applied Biosystems, Foster City, CA, USA). The resulting plasmid containing the thaumatin II gene was designated pCR2.1-TOPO/thaumatin II. The pCR2.1-TOPO/thaumatin II was digested by *Csp*45 I and *Xba* I, and ligated with the yeast shuttle vector pPIC6α previously digested with the same restriction enzymes. The plasmid was digested by *Pme* I and introduced into *Pichia* X-33 by electroporation as described previously [13].

Recombinant thaumatin II was expressed using a 7-L fermenter (TS-M7L; Takasugi Seisakusho Co., Tokyo, Japan) with controlled temperature and pH (FC-2000; Tokyo Rikakikai Co., Ltd.) as described previously [13,14]. The supernatant of the culture medium was dialyzed and the dialysate was applied to the SP-Sephadex column (GE Healthcare Bio-Science AB, Uppsala, Sweden). The bound proteins were eluted with 5 mM sodium phosphate buffer, pH 7.0 containing 0.5 M NaCl. The fractions containing thaumatin were collected and precipitated with 75% ammonium sulfate. The precipitate was collected by centrifugation at 8,000×g for 30 min, and dissolved in 20 mM Hepes buffer, pH 7.0, containing 150 mM NaCl, and further purified by gel-filtration chromatography (HW50F; Tosoh Co. Tokyo,

Japan).

2.3. Crystallization and data collection

The purified recombinant thaumatin II was concentrated by a VIVACON 2 (Sartorius Stedim Biotech GmbH, Goettingen, Germany), and the protein concentration was measured with a NanoDrop®ND-1000 spectrophotometer (NanoDrop Technologies, Inc., Rockland, DE, USA). A crystal of recombinant thaumatin II was obtained by the hanging-drop vapour-diffusion method at 293K. The hanging drops were prepared by mixing 5 μL of 30-50 mg/mL protein solution with 5 μL reservoir solution (0.1M N-(2-acetanido) iminodiacetic acid, 0.75 M potassium sodium tartrate and 12.5% glycerol, pH 7.0). The crystal was placed in a cold nitrogen gas stream and X-ray diffraction images were collected using an RAXIS-V area detector (Rigaku, Tokyo, Japan) with synchrotron radiation at a wavelength of 0.8 Å at the BL-26B1 station of SPring-8 (Hyogo, Japan). The data obtained were processed, merged, and scaled using the HKL2000 program package [15]. Data collection and structure solution statistics are shown in Table 1.

2.4. Structure refinement and validation

The structure of recombinant thaumatin II was determined with the

Shelxpro package [16] using the structure of plant thaumatin II (1.27 Å, PDB entry 3aok) as a reference [11]. Initial rigid body refinement and subsequent refinements were performed using the SHELXL97 and SHELXL-2013 program [16]. The models were rebuilt using the Coot program [17]. Water molecules were incorporated where the |Fo|-|Fc| electron density map showed peaks above 3σ and density above 1σ was present for the 2|Fo|-|Fc| map. All reflections were included with no σ cutoff; 5% of the data were randomly selected and omitted during refinement for cross validation by means of the free *R*-factor [18]. The occupancy of the major conformation was refined first, and then the second or third conformation was assigned and refined based on its |Fo|-|Fc| map. The occupancies of the disorders were treated as free variables and refined using the FVAR restraints. Anisotropic *B*-factor refinement was performed using the SHELXL package, and finally hydrogen atoms were generated based on the HFIX. Hydrogen atoms were included only in the protein atoms but not in tartrate/glycerol/solvent atoms. In order to estimate the standard deviations, an unrestrained refinement was attempted by setting the shift multiplication parameters to zero. The quality of the final model was assessed using PROCHECK [19] and RAMPAGE [20]. The CCP4 package was used for the manipulation of data and coordinates [21]. The electron density maps and structural images were generated using PyMOL [22]. The coordinates and observed intensities of recombinant thaumatin II

have been deposited in the PDBj (accession code 3wou).

3. Results and discussion

3.1. Crystallization and refinement statics of recombinant thaumatin II

We purified recombinant thaumatin II from the culture medium of the yeast *Pichia pastoris* and attempted its crystallization. Numerous pyramid and bipyramid-shaped small crystals were obtained in a few days. We next attempted to crystallize it in the presence of 12.5% (v/v) glycerol and the relatively large crystals (approximately 0.4 × 0.4 × 0.8 mm) for high resolution structural analysis appeared within two weeks. The crystals obtained in this condition belonged to space group $P4_12_12$ with a = b = 57.685 Å, c = 150.011 Å, α=β=γ= 90°. The number of total reflections and unique reflections for recombinant thaumatin II at 0.99 Å was 2,080,267 and 141,082, respectively, more than double those of plant thaumatin II at 1.27 Å (total reflections = 942,463 and unique reflections = 68,167) [11]. In an isotropic refinement, 8,808 parameters were used and the data to parameter ratio of the recombinant thaumatin II was 15.985 which was about twice that of plant thaumatin II (8.203) at 1.27Å. Anisotropic *B*-factor refinement was performed against the data up to a resolution of 0.99 Å, using 20,811 parameters against 140,800 unique reflections (the data to parameter ratio is 6.766), resulted in an

R_{work} of 11.53% and an R_{free} of 14.73%. Next, hydrogen atoms were modelled based on the HFIX, and the R_{work} and R_{free} fell to 9.70% and 11.85%, respectively. Using 20,908 parameters, the data to parameter ratio in this stage became 6.734. To finalize the refinement, the model including hydrogen atoms was refined against all data for 100 cycles using conjugate-gradient least squares minimization, leading to an *R*1 of 9.74% for 140,800 reflections and 9.16% for 128,395 reflections with $Fo > 4\sigma(Fo)$ in the range 10-0.99 Å (Table 1).

3.2. Overall structure of recombinant thaumatin II

The final model of recombinant thaumatin II consisted of 207 residues with 4,004 protein atoms, including 1,689 hydrogen atoms, 2 tartrate ions, 2 glycerol molecules, and 483 water molecules. Previous our results showed that 2 tartrate ions, 4 glycerol molecules and 476 water molecules were modelled in the recombinant thaumatin I (PDB: 3al7) [7]. The locations of tartrate ions as well as glycerol molecules in thaumatin II were almost same as those of thaumatin I. A Ramachandran plot calculated for the final model of the recombinant thaumatin II showed that 87.6% of the residues were in the most favoured regions, 11.8% were in additional allowed regions, and 0.6% were in generously allowed regions. No residues were in disallowed regions. One cis-peptide was formed in Pro84. The average *B* factors for α-carbon, side

chain and all protein atoms were 10.136 Å^2, 15.623 Å^2, and 14.153 Å^2, respectively. (Table 1). An unrestrained refinement was attempted and positional uncertainties were plotted against thermal parameters (supplemental Fig.1). The positional s.u. for carbon at B = 50 Å^2 was about 0.10 Å, and for B < 10 Å^2, the positional s.u. fell below 0.02 Å, indicating the accuracy of the model structure [23].

3.3. Amino acid residues in multiple conformations

In the structure of recombinant thaumatin II at 0.99 Å, an electron density map allowed the side chains of 24 residues (Thr2, Glu4, Leu31, Glu35, Lys49, Asp55, Tyr57, Arg67, Asp70, Lys78, Arg79, Arg82, Lys106, Met112, Arg119, Cys121, Val124, Gly143, Cys159, Lys163, Glu168, Arg171, Asp179 and Arg200) to be modelled in two conformations, and 2 residues (Arg122 and Ser155) to be modelled in three conformations (Fig. 1). In comparison to the structure of plant thaumatin II at 1.27 Å (PDB code 3aok, [11]), we could identify 5 disordered residues (Glu35, Asp55, Gly143, Arg171, and Arg200) in the high-resolution structure of recombinant thaumatin II (Fig. 1). These residues were located posterior to the cleft-containing region. Four charged residues (Glu35, Asp55, Arg171 and Arg200) were also identified in plant thaumatin I (PDB code 2vhk, [6], PDB code 3ald, [7]) and recombinant thaumatin I (PDB code 3al7, [7]). Notably, we could successfully identify two

conformations for G143 (occupancy was 0.58 for G143 (A) and 0.42 for G143 (B), respectively) (Fig. 2). The *B*-factors for the main chain of N atom, Cα atom, C atom, and O atom for Gly143 (A) was 19.34 $Å^2$, 16.64 $Å^2$, 12.44 $Å^2$, and 11.46 $Å^2$, respectively. And that for Gly143 (B) was 13.31 $Å^2$, 15.78 $Å^2$, 12.85 $Å^2$, and 10.93 $Å^2$, respectively. The backbone C=O atoms of G143 (A) and G143 (B) were 3.2 Å from each other. G143 was located in the centre of three consecutive glycine residues (G142-G143-G144) that are adjacent to R67 (Fig. 3C). C=O atoms of G142 formed hydrogen bonds with HB3 of R67, which is one of the sweetness determinants. As shown in Fig. 3A and 3B, the side-chains of the two critical residues of R67 and R82 were also disordered. The average *B*-factors for the side chains of R67 (A) and R67 (B) were 11.39 $Å^2$, and 12.05 $Å^2$, respectively, and those for the side chains of R82 (A) and R82 (B) were 11.72 $Å^2$, and 12.32 $Å^2$, respectively. Furthermore, the r.m.s. deviation of Cα atoms of G142 was relatively high, suggesting the likely backbone mobility of the three glycine residues (Fig. 4A). Taken together, the side chain in sweet determinants, as well as the backbone of three consecutive glycine residues were more disordered and contained alternative conformations.

3.4. Hydrogen-bond network in C-terminal regions and R8

Although R8 was modelled in two conformations with an occupancy of

0.83 for R8 (A) and 0.17 for R8 (B) in plant thaumatin II at 1.27 Å, no alternative conformation was assigned to recombinant thaumatin II at 0.99 Å. To clarify these discrepancies we further examined around R8 and revealed that the C-terminal regions of recombinant thaumatin II were quite different from those of plant thaumatin II (Fig. 5). C-terminal regions of recombinant thaumatin II were well fitted in the electron density map, and C-terminal A207 shifted to the nearby R8 and then formed hydrogen bonds with the side chains of R8 (Fig. 5). The distances of atoms less than 5.00 Å are shown in Table 2. In particular, the distances between O of R8 and HB2 of A207, O of R8 and HB3 of A207 were 2.88Å and 2.71Å, respectively, and the HD3 of R8 and OT2 of A207 was 2.83Å. By forming hydrogen bonds between R8 and Ala207, the mobility of the side chain of R8 might be reduced and only one conformation could be assigned to recombinant thaumatin II.

3.5. Comparison of the structure of plant thaumatin II (1.27 Å)

The differences in r.m.s. deviation on Cα atoms as well as side-chain atoms between the final refined structure of recombinant thaumatin II (0.99 Å, PDB code 3wou) and that of plant thaumatin II (1.27 Å, PDB code 3aok) were investigated (Fig. 4). The most notable difference was found in a C-terminal residue A207 for Cα atoms (2.71 Å) and side-chain atoms (5.55 Å). Nine residues (N32, D60, R67, R82, R119, R122, N146, K163, and A207) had an

r.m.s.d. value more than 1.5 Å for side-chain atoms. Among them, five residues (R67, R82, R119, R122 and K163), including two critical residues for sweetness (R67 and R82), were modelled in two conformations or three conformations, suggesting that these residues have flexible conformations. The faint electron density around D60 might have resulted in a high r.m.s.d. value. The electron density maps of the remaining two residues (N32 and N146) were further examined and found that the locations of ND2 and OD1 were reversed to OD1 and ND2, respectively, when compared to plant thaumatin II at 1.27 Å.

Although the structural requirements necessary for the sweetness of thaumatin molecules have been investigated [9, 10, 24-26], the three-dimensional structure of sweet receptors T1R2-T1R3 has not yet been determined. Various models of the interaction between sweet receptors and sweet-tasting proteins have been proposed by considering and referring to the structural as well as mutagenesis results [2, 3, 27-30]. Information about the detailed structure of sweet-tasting proteins would be useful for revealing how the ligand-binding site of sweet receptors confers a broad and/or specific receptive range.

In conclusion, atomic resolution structural analyses of thaumatin II revealed flexible conformations of the side chains of critical residues as well as three consecutive glycine residues (G142-G143-G144) located adjacent to

R67. Insights into the detailed structural features of recombinant thaumatin II with hydrogen atoms obtained in this study will provide important information on the perception of the sweet taste of thaumatin and the molecular mechanism by which thaumatin activates sweet receptors.

Acknowledgements

This work was supported by a Grant-in-Aid for Young Scientists (B) (T.M., no.19780074) and Scientific Research (C) (T.M., no. 22580105, 25450167) from The Japan Society for the Promotion of Science and by the Japan Food Chemical Research Foundation. The synchrotron radiation experiments were performed at BL26B1 in SPring-8 with the approval of the Japan Synchrotron Radiation Research Institute (JASRI) (proposal numbers 2010A6538, 2011A1417, 2011B1073, 2011B1404, 2012A1048, 2012B1067, 2012B1539).

References

[1] H. van der Wel, K. Loeve, Isolation and characterization of thaumatin I and II, the sweet-tasting proteins from Thaumatococccus daniellii Benth, *Eur. J. Biochem.* **31** (1972) 221–225.

[2] P.A. Temussi, Why are sweet proteins sweet? Interaction of brazzein,

monellin and thaumatin with the T1R2-T1R3 receptor, FEBS Lett. 526 (2002) 1–4.

[3] P.A. Temussi, Natural sweet macromoleculars: how sweet protein work, Cell Mol. Life Sci. 63 (2006) 1876–1888.

[4] K. Ohta, T. Masuda, F. Tani, N. Kitabatake, The cysteine-rich domain of human T1R3 is necessary for the interaction between human T1R2–T1R3 sweet receptors and a sweet-tasting protein, thaumatin, Biochem. Biophys. Res. Commun. 406 (2011) 435–438.

[5] T. Masuda, W. Taguchi, A. Sano, K. Ohta, N. Kitabatake, F. Tani, Five amino acid residues in cysteine–rich domain of human T1R3 were involved in the response for sweet-tasting protein thaumatin, Biochimie, 95 (2013) 1502–1505.

[6] N. Asherie, J. Jakoncic, C. Ginsberg, A. Greenbaum, V. Stojanoff, B.J. Hrnjez, S. Blass, J. Berger, Tartrate chirality determines thaumatin crystal habit, Cryst. Growth Des. 9 (2009) 4189–4198.

[7] T. Masuda, K. Ohta, B. Mikami, N. Kitabatake, High-resolution structure of the recombinant sweet-tasting protein thaumatin I, Acta Crystallogr. Sect. F67 (2011) 652–658.

[8] T. Masuda, K. Ohta, B. Mikami, N. Kitabatake, F. Tani, Atomic structure of the sweet-tasting protein thaumatin I at pH8.0 reveals the large

disulfide-rich region in domain II to be sensitive a pH change, Biochem. Biophys. Res. Commun. 419 (2012) 72–76.

[9] S.C. Teixeira, M.P. Blakeley, R.M. Leal, E.P. Mitchell, V.T. Forsyth, A preliminary neutron crystallographic study of thaumatin, Acta Crystllogr. Sect. F64 (2008) 378–381.

[10] S.C. Teixeira, M.P. Blakeley, R.M. Leal, S.M. Gillespie, E.P. Mitchell, V.T. Forsyth, Sweet neutron crystallography, Acta Crystllogr. Sect. D66 (2010) 1139–1143.

[11] T. Masuda, K. Ohta, F. Tani, B. Mikami, N. Kitabatake, Crystal structure of the sweet-tasting protein thaumatin II at 1.27Å, Biochem. Biophys. Res. Commun. 410 (2011) 457–460.

[12] T. Masuda, S. Tamaki, R. Kaneko, R. Wada, Y. Fujita, A. Metha, N. Kitabatake, Cloning, expression and characterization of recombinant sweet-protein thaumatin II using the methylotrophic yeast *Pichia pastoris*, Biotechnol. Bioeng. 85 (2004) 761–769.

[13] T. Masuda, Y. Ueno, N. Kitabatake, High yield secretion of the sweet-tasting protein lysozyme from the yeast Pichia pastoris, Protein Expr. Purif. 39 (2005) 35–42.

[14] T. Masuda, N. Ide, K. Ohta, N. Kitabatake, High-yield secretion of the recombinant sweet-tasting protein thaumatin I, Food Sci. Technol. Res.

16 (2010) 585–592.

[15] Z. Otwinowski, W. Minor, Processing of X-ray crystallographic data collected in oscillation mode, Methods Enzymol. 276 (1997) 307–326.

[16] M. Sheldrick, T.R. Schneider, SHELXL: high-resolution refinement, Methods Enzymol. 277 (1997) 319–343.

[17] P. Emsley, K. Cowtan, Coot: model-building tools for molecular graphics, Acta Crystllog. Sect. D60 (2004) 2126–2132.

[18] A.T. Brünger, Free R value: a novel statistical quantity for assessing the accuracy of crystal structures. Nature, 355, (1992) 472–475.

[19] R.A. Laskowski, M.W. MacArthur, D.S. Moss, J. M. Thornton, PROCHECK: a program to check the stereochemical quality of protein structures, J. Appl. Cryst. 26 (1993) 283–291.

[20] S.C. Lovell, I.W. Davis, W.B. Arendall III, P.I.W. de Bakker, J.M. Word, M.G. Prisant, J.S. Richardson, D.C. Richardson, Structure validation by Cα geometry: φ, ψ and Cβ deviation, Proteins, 50, 437–450.

[21] M.D. Winn, C.C. Ballard, K.D. Cowtan, E.J. Dodson, P. Emsley, P.R. Evans, R.M. Keegan, E.B. Krissinel, A.G.W, A. McCoy, S.J. McNicholas, G.N. Murshudov, N.S. Pannu, E.A. Potterton, H.R. Powell, R.J. Read, A. Vagin, K.S. Wilson, Overview of the CCP4 suite and current developments, Acta Crystllog. Sect. D67 (2011) 235–242.

[22] W.L. DeLano, (2002). The PyMOL Molecular Graphics System. DeLano Scientific, San Carlos, CA, USA. 2002.

[23] D.W.J. Cruickshank, Remarks about protein structure precision, Acta Crystllog. Sect. D55 (1999) 583–601.

[24] S.H. Kim, J.L. Weickmann, Crystal structure of thaumatin I and its correlation to biochemical and mutation studies, in: M. Witty, J.D. Higginbotham (Eds.), Thaumatin, CRC Press, Boca Raton Florida, 1994, pp. 135–149.

[25] K. Ohta, T. Masuda, N. Ide, N. Kitabatake, Critical molecular regions for elicitation of the sweetness of the sweet-tasting protein thaumatin I, FEBS J. 275 (2008) 3644–3652.

[26] K. Ohta, T. Masuda, F. Tani, N. Kitabatake, Introduction of a negative charge at Arg82 in thaumatin abolished responses to human T1R2-T1R3 sweet receptors, Biochem. Biophys. Res. Commun. 413 (2011) 41–45.

[27] A. Shimizu-Ibuka, Y. Morita, T. Terada, T. Asakura, K. Nakajima, S. Iwata, T. Misaka, H. Sorimachi, S. Arai, K. Abe, Crystal structure of neoculin: insight into its sweetness and taste-modifying activity, J. Mol. Biol. 359 (2006) 148-158.

[28] M. Cui, P. Jiang, E. Maillet, M. Max, R.F. Margolskee, R. Osman, The heterodimeric sweet taste receptor has multiple potential ligand binding sites, Curr. Pharm. Des. 12 (2006) 4591-4600.

[29] D.E. Walters, T. Cragin, Z. Jin, J.N. Rumbley, G. Hellekant, Design and evaluation of new analogs of the sweet protein brazzein, Chem. Senses 34 (2009) 679-683.

[30] F.M. Assadi-Poter, E.L. Maillet, J.T. Radek, J. Quijada, J.L. Markley, M. Max, Key amino acid residues involved in multi-point binding interactions between brazzein, a sweet protein, and the T1R2-T1R3 human sweet receptor, J. Mol. Biol. 398 (2010) 584-599.

Figure legends

Figure 1. **Alternative side-chain conformations in recombinant thaumatin II at 0.99 Å.**

In comparison to the structure of plant thaumatin II at 1.27 Å, the residues modelled in two conformations only for recombinant thaumatin II are shown in blue and the residues modelled in two conformations, both recombinant and plant, are shown in green. The residues modelled in three conformations are shown in red. Residues R67 and R82, which are critical for sweetness, are shown in cyan.

Figure 2. Gly143 modelled in two conformations.

The σA-weighted 2mFo-DFc maps contoured at 1.0σ are shown in blue and mFo-DFc maps omitting hydrogen atoms contoured at 3.0σ and -3.0σ are shown in green and red, respectively.

Figure 3. **The model and electron density for recombinant thaumatin around Arg67, and Arg82.**

The OMIT maps are shown in (A) Arg67. (B) Arg82. The σA-weighted 2mFo-DFc maps contoured at 1.0σ are shown in blue and mFo-DFc maps omitting hydrogen atoms contoured at 3.0σ are shown in green. (C) The

models around Arg67, Gly142, Gly143, and Gly144. Gly143 is modelled in two conformations. The main chain atoms for Gly142, Gly143 and Gly143 are shown in stick model and indicated in red, cyan, and yellow, respectively.

Figure 4. **R.m.s.d values of Cα atoms and side chain.**

The superposition of the coordinates of the Cα atoms and side chain of recombinant thaumatin II at 0.99 Å onto plant thaumatin II at 1.27 Å. Histograms of r.m.s. d. values of Cα atoms (A) and side chain (B) with the residue number.

Figure 5. **Hydrogen-bond network between C-terminal regions and Arg8.**

The model and electron density around C-terminal regions and Arg8.

The OMIT maps are shown in (A). The σA-weighted 2mFo-DFc maps contoured at 1.0σ are drawn in blue and the mFo-DFc maps omitting hydrogen atoms contoured at 3.0σ and -3.0σ are shown in green and red, respectively. (B) Comparison of the model of recombinant thaumatin II at 0.99 Å and plant thaumatin II at 1.27 Å. The stick models of recombinant thaumatin II and plant thaumatin II are shown in blue and red, respectively. The distances less than 3.0 Å are indicated in the dashed lines (Table 2).

Supplementary Figure 1.

E.s.d. analysis of the recombinant thaumatin II at 0.99Å.

Plot of positional e.s.d. versus the thermal parameter for C atoms (black), N atoms (cyan), and O atoms (red), respectively.

Table 1. Data collection and refinement

Data collection	
Beamline	**SPring-8 BL26B1**
Detector	**R-AXISV**
Crystal systems	**Tetragonal**
Space group	**$P4_12_12$**
Cell dimension (Å, °)	**a = 57.685, b = 57.685, c = 150.011, $\alpha = \beta = \gamma = 90$**
X-ray wavelength (Å)	**0.80**
Resolution limit (Å)	**50.0-0.99 (1.01-0.99)**
Total reflections	**2080267**
Unique reflections	**141082**
R_{merge}	**0.069 (0.496)**
Completeness (%)	**99.8 (100)**
Redundancy	**8.9 (8.1)**
$\langle I \rangle / \langle \sigma(I) \rangle$	**64.34 (6.26)**
Refinement	
Resolution (Å)	**10-0.99**
Unique reflections	**133756 (Fo>4σ:121966)**
Parameter ratio	**6.870**
R_{work}/R_{free}	**9.70/11.85 (9.12/11.23)**
Unique reflections	**140800 (Fo>4σ:128395)**
Parameter ratio	**6.734**
R_{cryst}	**9.74 (9.16)**
Average B factor (4004 atoms)	**16.667**
Protein (3489 atoms)	**14.153**
Tartrate (20 atoms)	**12.592**
Glycerol (12 atoms)	**55.149**
Water (483 atoms)	**34.044**
R.m.s.deviation from ideal value	
r.m.s.d bond (Å)	**0.0182**
r.m.s.d angle (Å)	**0.0389**
Ramachandran plot (%)	
Most favoured	**87.6**
Additional allowed	**11.8**
Generously allowed	**0.6**
Disallowed	**0**
Matthews coefficient Vm ($Å^3$/Da)	**2.80**
Solvent content (%)	**56.09**

Table 2. Distances between Arg8 and Ala207 or Pro205

Atom 1	Atom 2	Distance (Å)
Arg8 O	Ala207 HB3	2.71
Arg8 O	Ala207 HB2	2.88
Arg8 O	Ala207 HB1	3.60
Arg8 HG3	Ala207 OT2	3.53
Arg8 HG3	Ala207 OT1	4.31
Arg8 HD3	Ala207 OT2	2.83
Arg8 HD2	Pro205 N	4.09

Figure 1

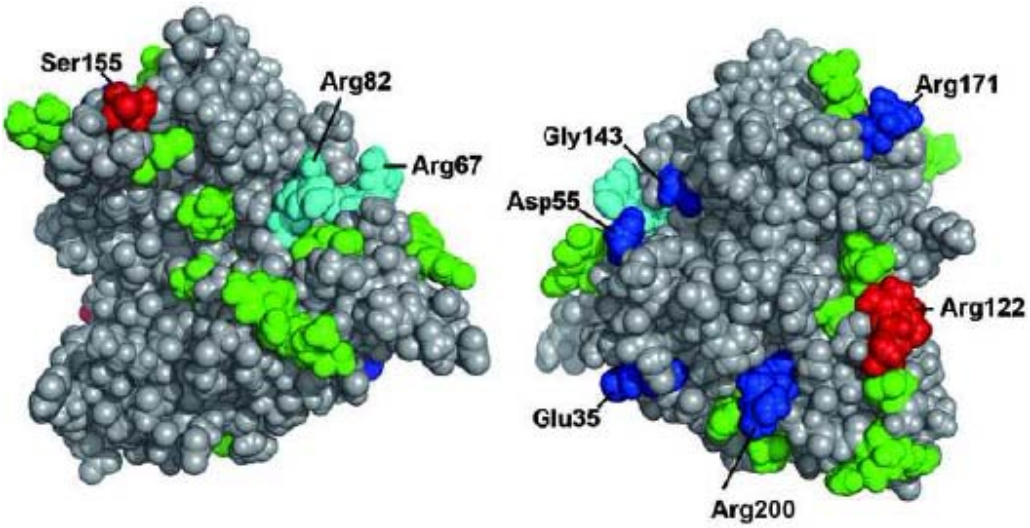
Ser155
Arg82
Arg67
Gly143
Arg171
Asp55
Arg122
Glu35
Arg200

Figure 2

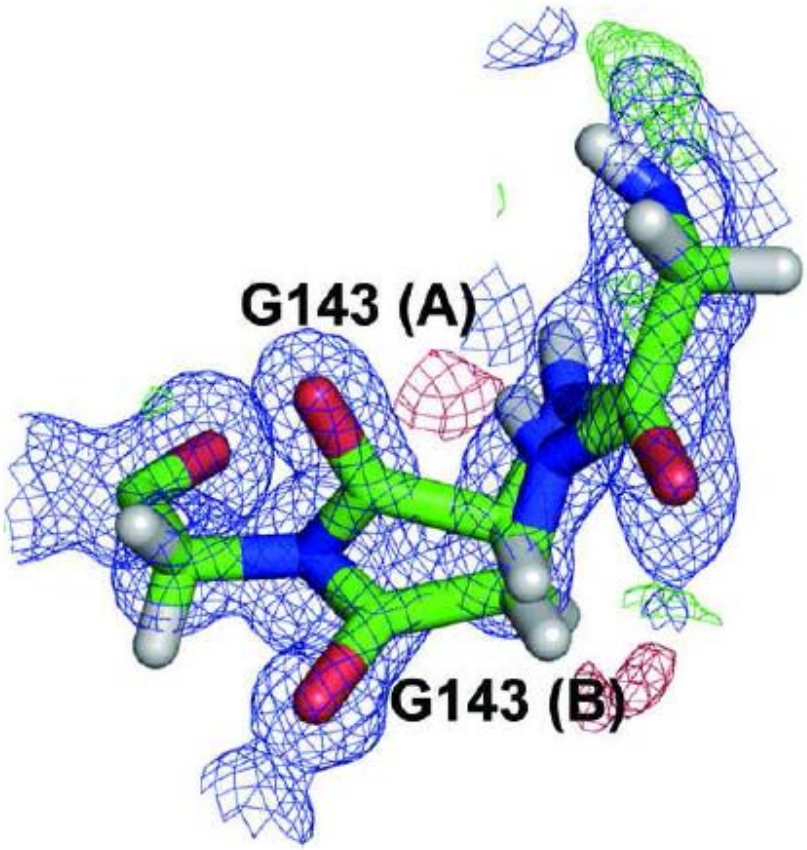

Figure 3

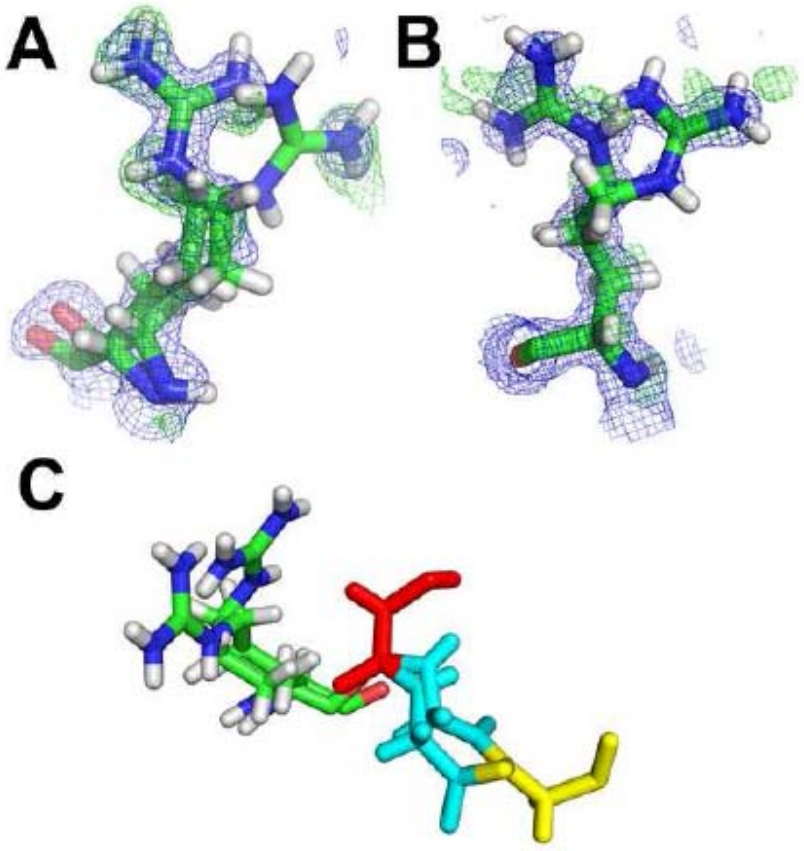

Figure 4

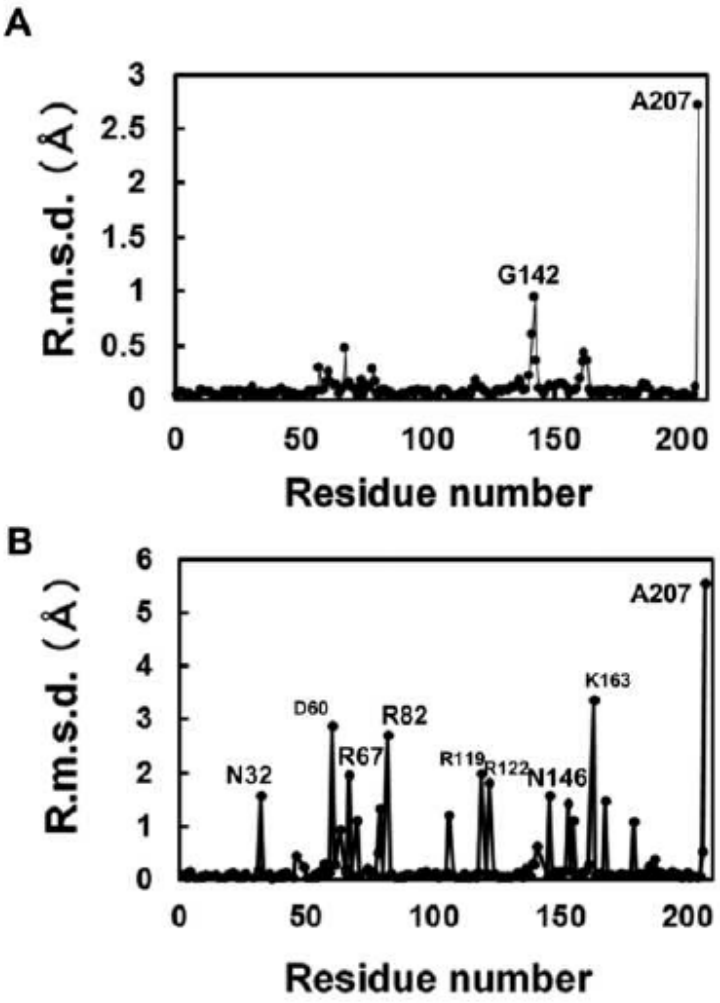
A
R.m.s.d. (Å)
3
2.5
2
1.5
1
0.5
0
A207
G142
0
50
100
150
200
Residue number
B
R.m.s.d. (Å)
6
5
4
3
2
1
0
A207
K163
D60
R82
R67
N32
R119
R122
N146
0
50
100
150
200
Residue number

Figure 5

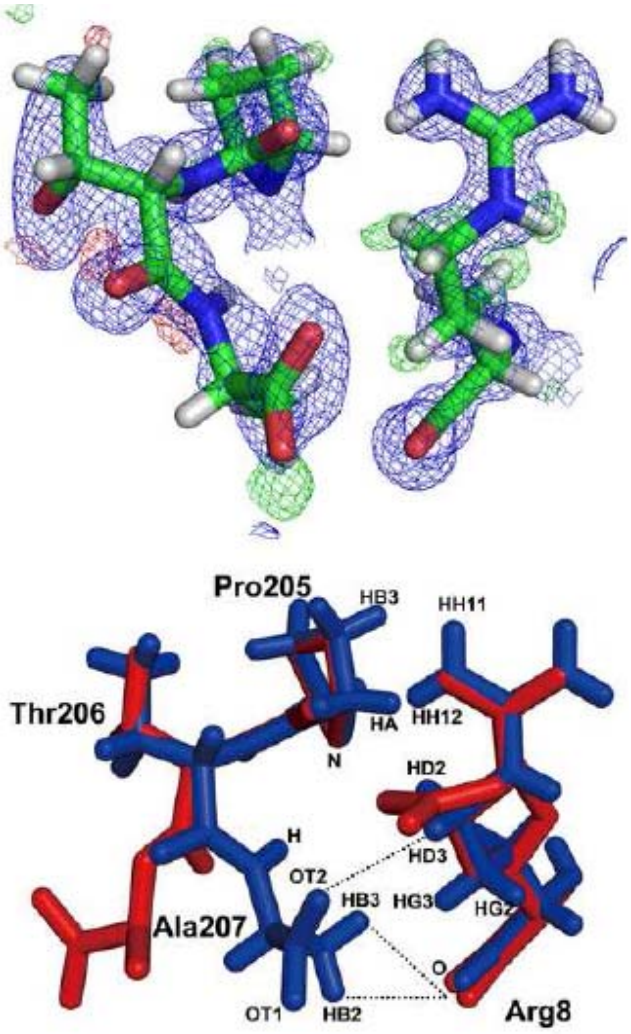
Pro205
HB3
HH11
Thr206
HA
HH12
N
HD2
H
HD3
OT2
HB3
HG3
HG2
Ala207
O
OT1
HB2
Arg8

Supplementary Figure 1